JCTC Journal of Chemical Theory and Computation

pubs.acs.org/JCTC Article

Grand Canonical Ensemble Modeling of Electrochemical Interfaces Made Simple

Zhaoming Xia and Hai Xiao*

Cite This: https://doi.org/10.1021/acs.jctc.3c00237 Read Online

ACCESS | Metrics & More | Article Recommendations | Supporting Information

ABSTRACT: Grand canonical ensemble (GCE) modeling of electrochemical interfaces, in which the electrochemical potential is converged to a preset constant, is essential for understanding electrochemistry and electrocatalysis at the electrodes. However, it requires developing efficient and robust algorithms to perform practical and effective GCE modeling with density functional theory (DFT) calculations. Herein, we developed an efficient and robust fully converged constant-potential (FCP) algorithm based on Newton's method and a polynomial fitting to calculate the necessary derivative for DFT calculations. We demonstrated with the constant-potential geometry optimization and Born−Oppenheimer molecular dynamics (BOMD) calculations that our FCP algorithm is resistant to the numerical instability that plagues other algorithms, and it delivers efficient convergence to the preset electrochemical potential and renders accurate forces for updating the nuclear positions of an electronically open system, outperforming other algorithms. The implementation of our FCP algorithm enables flexibility in using various computational codes and versatility in performing advanced tasks including the constant-potential enhanced-sampling BOMD simulations that we showcased with the modeling of the electrochemical hydrogenation of CO, and it is thus expected to find a wide spectrum of applications in the modeling of chemistry at electrochemical interfaces.

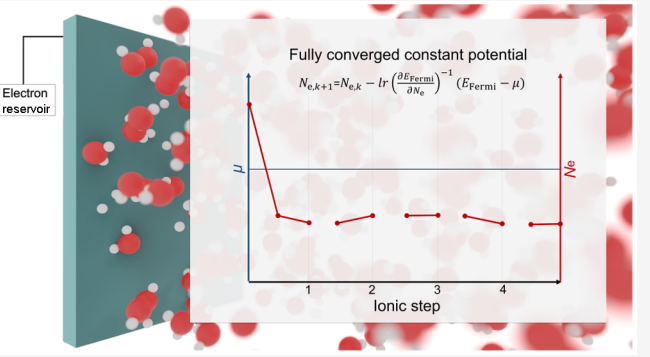

1. INTRODUCTION

Approximate methods based on density functional theory (DFT)[1] have been widely employed to calculate the energies and forces of chemical systems at the atomic level, and the time evolution of chemical systems can be further modeled with the Born−Oppenheimer (BO) approximation.[2] Among various types of chemical systems, the electrochemical interfaces are of fundamental interest and crucial importance to guide the design of electrocatalysis, yet they pose challenges for DFT calculations,[3−5] one of which is the modeling of applied potentials.

The constant-charge approach, in which the total number of electrons (N_e) is kept constant, has been widely adopted in the DFT calculations for electrochemistry, and the contribution of the applied potential is taken into account implicitly as a correction to the reaction free energy using the computational hydrogen electrode (CHE) method.[6] These calculations normally assume the potential of zero charge (PZC) for the electrochemical interfaces, while modification of the potential can be achieved by introducing compensating counter charges or hydrated ions with explicit solvent molecules.[7−10] Nevertheless, the electrochemical potential cannot be kept constant because N_e is not allowed to vary during the structural evolution, particularly in the constant-charge BO molecular dynamics (BOMD) simulations. This does not jibe with the realistic scenarios, in which N_e should adapt to the applied constant potential and thus vary with the nuclear motions. Therefore, the constant-charge approach is not precise for modeling the electrochemical interfaces.

The introduction of implicit electrolyte models enables continuous variation in N_e of the electrode system and a more realistic description of the electrochemical double layer in a computationally efficient way.[11−16] Thus, the constant-potential approach, i.e., the grand canonical ensemble (GCE) approach,[16−20] can be made feasible by introducing the implicit electrolyte model, and the grand free energy of electronic system at a specified potential is optimized with respect to N_e together with the electron density. Nevertheless, solving the Kohn−Sham equations with N_e as an additional variable requires algorithms beyond the self-consistent field (SCF) method for numerical stability,[16,18] which are not widely implemented. Therefore, there have been efforts made to develop algorithms for updating N_e external to the SCF convergence of constant-charge electron density,[15,21−25] in

Received: February 28, 2023

pursuit of the flexibility in using various DFT codes as well as the computational efficiency for demanding tasks such as the constant-potential BOMD simulations.

In particular, Bonnet et al. introduced a fictitious force acting on N_e to drive the convergence to a preset electrochemical potential in the MD simulations, i.e., with a fictitious potentiostat.[21] Zhao et al. conducted the constant-potential MD simulations by updating N_e every few MD steps based on the constant-capacitance assumption, in order to reduce the computational complexity.[24] Deißenbeck et al. included the two counter electrodes in the modeling systems and thus formulated a thermopotentiostat approach to perform constant-potential MD simulations under the canonical ensemble; i.e., N_e of the modeling system remains constant.[26,27] In these approaches, the electrochemical potential fluctuates around a constant average, and the constant-potential properties can be obtained by taking averages. Very recently, Melander et al. developed the constant inner potential (CIP) method as a more robust and general approach for performing constant-potential modeling that can be extended to the scenarios where the Fermi level from DFT calculations does not reflect the experimental electrode potential.[28]

With the implicit electrolyte model that ensures the charge neutrality of a modeling system, N_e can be continuously updated to converge precisely to a constant potential at each nuclear step, which we term as a fully converged constant-potential (FCP) approach. However, the FCP approach requires the electrochemical potential to converge precisely to a preset value in every nuclear step, which may greatly increase the computational complexity. Therefore, developing an efficient and robust FCP algorithm is essential for practical and effective FCP modeling of electrochemical interfaces. We note that the fluctuation of potential controlled by a potentiostat is necessary for constant-potential MD simulations,[26,27,29] and a general FCP algorithm should have the flexibility to include such capability.

In this work, we formulated and implemented a new FCP algorithm based on Newton's method and a polynomial fitting to calculate the necessary derivative, and it is external to the SCF calculations, thus providing the flexibility in using various computational codes. We performed benchmark constant-potential calculations to demonstrate that this simple FCP algorithm is resistant to the numerical instability arising from common convergence calculations of electronic states that plague other algorithms, and it is able to deliver efficient convergence to the preset electrochemical potential and renders accurate forces for updating the nuclear positions of an open system, outperforming other algorithms. We further showcased the versatility of our FCP implementation to perform constant-potential enhanced-sampling BOMD simulations.

2. FORMULATION AND IMPLEMENTATION

Without the presence of an external field other than that generated by the nuclei, the grand free energy of an electronically open system (Ω) is a functional of the nuclear coordinates ($\vec{r}_n$), the electronic density (ρ), and the electrochemical potential (μ) set by the electron reservoir.[30,31] However, in the practical implementation of GCE-DFT calculations, μ is given as a constant parameter instead of a variable, and thus we can effectively write $\Omega(\vec{r}_n, \rho)$. In addition, we focus here on the scheme in which ρ is optimized to the ground state at a constant N_e by the constant-charge SCF method and N_e is optimized in an outer loop to minimize Ω. The constant-charge SCF calculation gives the Helmholtz free energy (A) readily minimized to its electronic ground state at constant N_e and the Ω to minimize is

$$\Omega(\vec{r}_n, N_e) = A(\vec{r}_n, N_e) - (N_e - N_{e,PZC})\cdot\mu \quad (1)$$

where $N_{e,PZC}$ is the number of electrons at PZC. Note that all the energies are referenced to the vacuum level, and the applied potential (U) at the standard hydrogen electrode (SHE) scale corresponding to μ is calculated as $U = (\mu_{SHE} - \mu)/e$, where μ_{SHE} is the absolute electrochemical potential of SHE.[32]

To obtain the ground-state Ω at the given μ, we simply minimize eq 1 with respect to N_e, and this gives

$$\frac{\partial\Omega}{\partial N_e} = \frac{\partial A}{\partial N_e} - \mu = E_{Fermi} - \mu = 0 \quad (2)$$

where E_{Fermi} is the Fermi level of the closed system. With this condition met at every nuclear step, Ω is minimized to the electronic ground state of the open system, and we can then calculate the correct ground-state forces on nuclei ($\vec{F}$) by taking the derivative of eq 1 as

$$\vec{\nabla}\Omega = \vec{\nabla}A \quad (3)$$

where $\vec{\nabla}$ is the nabla operator with respect to $\vec{r}_n$, and $\vec{F} = -\vec{\nabla}\Omega = -\vec{\nabla}A$; i.e., they are exactly the same as the ground-state forces on nuclei in the closed system with N_e that minimizes Ω (i.e., $E_{Fermi} = \mu$), consistent with previous reports.[33,34] Therefore, it is practically essential for the FCP modeling to develop an algorithm that converges N_e at every nuclear step to minimize Ω with $E_{Fermi} = \mu$ precisely and efficiently; i.e., $|E_{Fermi} - \mu|$ can be converged to within a tight threshold with an affordable computational cost.

Here, we adopt the simple Newton's method for this one-dimensional optimization problem, and N_e in the iteration is updated with the following set of formulas:

$$H \equiv \frac{\partial^2\Omega}{\partial N_e^2} = \frac{\partial E_{Fermi}}{\partial N_e} \quad (4)$$

$$N_{e,k+1} = N_{e,k} - \frac{\partial\Omega}{\partial N_e}\Big/H = N_{e,k} - H^{-1}(E_{Fermi} - \mu) \quad (5)$$

where H is the second derivative of Ω with respect to N_e and can be calculated with eq 4 as the first derivative of E_{Fermi}; $N_{e,k}$ and $N_{e,k+1}$ are the numbers of electrons in the kth and the $(k+1)$th FCP steps, respectively.

However, there is no analytic form of H or E_{Fermi} from the Kohn−Sham formulation of DFT (KS-DFT), and the numerical approach to calculate H with a small finite difference of N_e (ΔN_e) approximating the denominator in eq 4 can lead to enormous amplification of numerical errors from the SCF convergence to solve KS-DFT. As a result, the numerical evaluation of H relies heavily on the SCF convergence threshold and can be extremely inaccurate, as shown in Figure S1. The errors of H are outrageous with the commonly used SCF convergence threshold of 10^{-5} eV (Figure S1b) and remain significant with a tight threshold of 10^{-7} eV (Figure S1c). Consequently, the inaccurate H greatly compromises the convergence efficiency of these second-derivative-based optimization algorithms. Although the accuracy of H can be improved by further reducing the SCF convergence threshold,

https://doi.org/10.1021/acs.jctc.3c00237
J. Chem. Theory Comput. XXXX, XXX, XXX−XXX

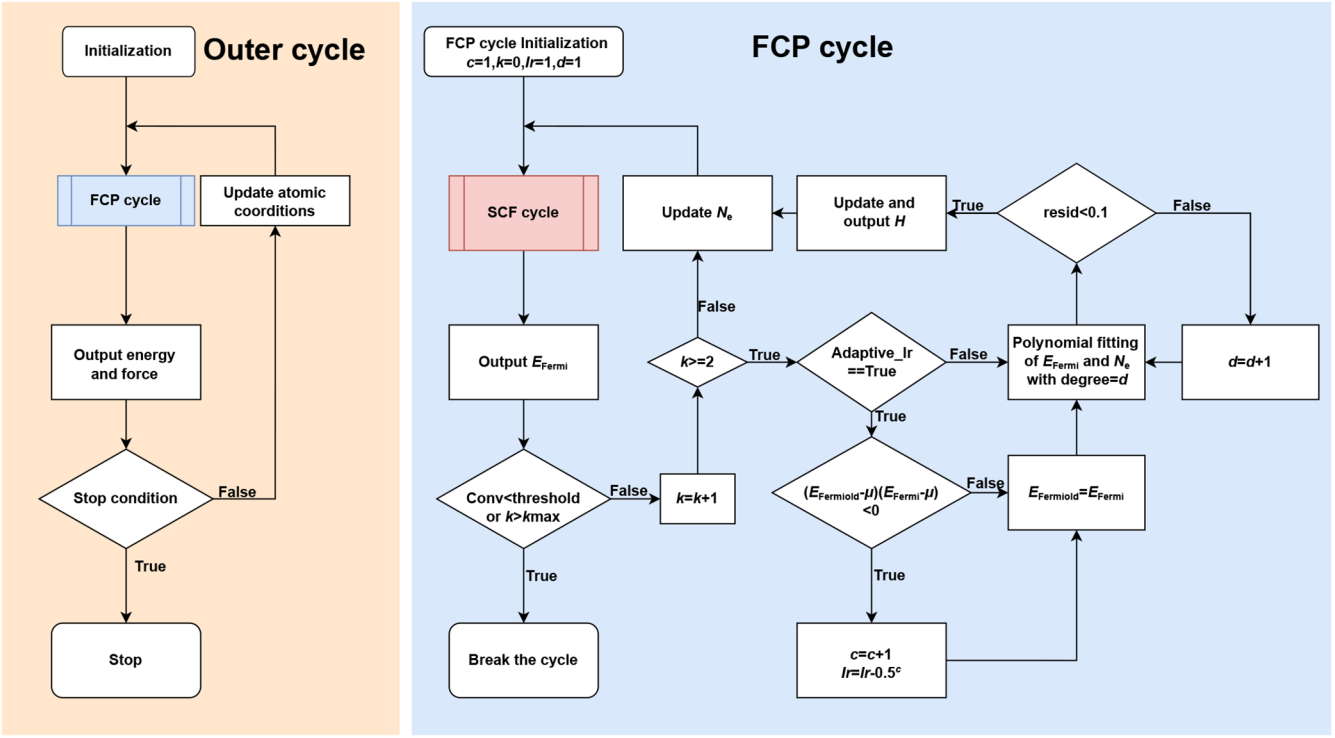

Figure 1. Flowchart of the FCP algorithm. The convergence criterion ("Conv") is defined as $|E_{Fermi} - \mu|$; k denotes the kth step in the iteration; $k$max is the maximal number of allowed steps; "Adaptive_lr" is the logic switch for introducing the learning rate to damp the oscillation; c marks the cth oscillation step; the residual error of the polynomial fitting is denoted as "resid".

it will dramatically increase the computational cost to converge the electronic state.

Inspired by the previously reported N_e–U curve and the constant-capacitance approximation,[21,24] we propose that the E_{Fermi}–N_e relationship can be well approximated as a monotonic smooth function by a polynomial fit, and then H in eq 4 can be calculated by simply taking the analytical first derivative of the polynomial-fitted function of the E_{Fermi}–N_e relationship. The numerical instability shown in Figure S1 may affect the residual of fitting, but it has a very limited impact on the fitted gradient. Thus, the new set of formulas for updating the iteration is

$$H^{\text{fitted}} = \frac{\partial E_{\text{Fermi}}^{\text{fitted}}(N_e)}{\partial N_e} \tag{6}$$

$$N_{e,k+1} = N_{e,k} - \text{lr}\cdot(H^{\text{fitted}})^{-1}(E_{\text{Fermi}}^{\text{fitted}}(N_e) - \mu) \tag{7}$$

where $E_{\text{Fermi}}^{\text{fitted}}(N_e)$ is the fitted function and lr is a learning-rate parameter that is introduced to damp possible oscillations during the iteration. Our FCP algorithm is then based on this simple approximation, and its flowchart is depicted in Figure 1.

In the FCP cycle, the E_{Fermi}–N_e relationship is initially polynomial fitted with the degree of the polynomial (d) equal to 1 (i.e., a linear fitting), and the fitting quality is evaluated by the residual error. If the residual error is over 0.1 eV, then d is increased for the polynomial fitting until the residual error is less than 0.1 eV. N_e is then updated by eqs 6 and 7. For certain special cases, N_e oscillates during the iteration, and it is hard to converge. An exponentially decaying learning rate (lr in eq 7) is thus introduced to damp the oscillation when it occurs.

Based on the Python framework of the atomic simulation environment (ASE),[35] we built an interface using the Vienna Ab initio Simulation Package (VASP)[36−39] as the calculator to showcase our FCP algorithm. Our implementation is available at https://github.com/hellozhaoming/FCP-vasp-ase. This can be readily extended to using other suitable computational packages as the calculator.

The implicit electrolyte models we used in the following calculations include the one based on the linearized Poisson–Boltzmann equation implemented in VASPsol,[40,41] the polarizable continuum model (PCM) of GLSSA13[42] in JDFTx,[18,43] and the solvated jellium method (SJM)[20,25,28] in GPAW.[44] The dielectric constant of the water solvent is set to 78.4. The effective surface tension of the cavity is ignored. A concentration of monovalent electrolyte of 1.0 mol/L is used, which corresponds to a Debye length of 3.0 Å.

3. RESULTS AND DISCUSSION

3.1. Basic Benchmark. We first benchmark the computational efficiency of our FCP algorithm for converging $|E_{Fermi} - \mu|$, in comparison with the widely recognized conjugate gradient (CG) algorithm and the Broyden–Fletcher–Goldfarb–Shanno (BFGS) algorithm. The benchmark calculations were conducted with a series of three-layer p(2 × 2) fcc(111) surfaces of late transition metals (Fe, Co, Ni, Cu, Ru, Rh, Pd, Ag, Os, Ir, Pt, Au), and all the slab models were fixed at the structures optimized under corresponding PZCs, in order to first focus on only the convergence of electronic states for open systems. The initial guess of N_e and H are first set to $N_{e,\text{PZC}}$ and $\frac{80}{S_{\text{Slab}}/\text{Å}^2}$ eV, a set of empirical values we found to be viable initial guesses for most of the cases. In order to contain the effect of numerical instability, we first test a tight SCF threshold of 10^{-7} eV, and Figure S2 shows that the FCP algorithm requires the same or slightly fewer numbers of steps to converge $|E_{Fermi} -$

https://doi.org/10.1021/acs.jctc.3c00237
J. Chem. Theory Comput. XXXX, XXX, XXX−XXX

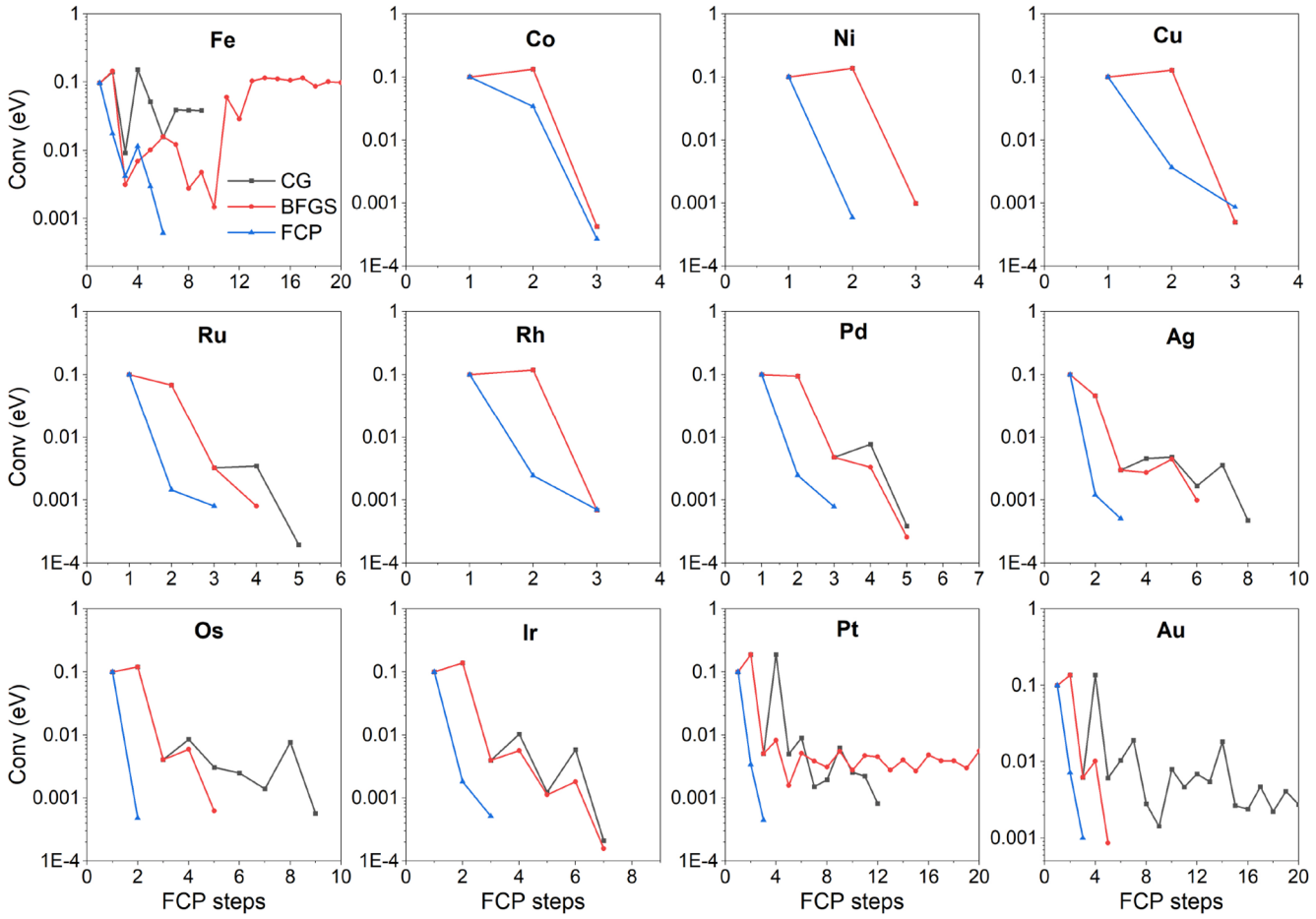

Figure 2. Benchmark calculations of late transition metal fcc(111) surfaces at U = 0.4 V with FCP, CG, and BFGS algorithms. The educated initial guesses of N_e and H are the calculated values at U = 0.5 V. The common SCF threshold of 10^{-5} eV is used. Adaptive_lr is true for Fe and false for other cases.

μ|, compared to the CG and BFGS algorithms. Nevertheless, we note that N_e in the FCP algorithm rapidly approaches the converged value within the very first few steps (Figure S3), which makes the SCF of later steps converge much faster because of good initial guesses of electronic densities. In contrast, the CG and BFGS algorithms require a line search to determine how far to move in the chosen direction, and this leads to relatively larger deviations of N_e in the first few steps (Figure S3), which are unfavorable for the SCF convergence in later steps.

In the common practices of FCP geometry optimization or BOMD, most FCP steps can use a set of educated initial guesses of N_e and H from the previous steps. Thus, we further test this common scenario where the FCP calculations start with a set of educated initial guesses of N_e and H. The results in Figure S4 show that the educated initial guesses slightly accelerate the convergences for all algorithms in general, and the FCP algorithm remains slightly better to converge than the CG and BFGS algorithms. We note that an educated initial guess of N_e may result in a side effect for CG and BFGS; i.e., it is too close to the converged value and the small ΔN_e amplifies the numerical errors for the SCF calculations. For example, it becomes difficult for CG or BFGS to converge for the Pd and Ag cases (Figure S4) because of the numerical instability. In contrast, the FCP algorithm is resistant to this side effect and shows little numerical instability, because the numerical errors are smoothed out by the polynomial fitting and this retains an accurate evaluation of H in Newton's iteration.

In addition, the tight SCF threshold of 10^{-7} eV tested above is computationally expensive. For example, the SCF calculations of Fe cases in Figures S2 and S4 require a few hundred SCF cycles to converge to within the tight threshold of 10^{-7} eV. Thus, we test the much more commonly used SCF threshold of 10^{-5} eV and find that this increases the numerical instability significantly. Consequently, Figure 2 shows that calculations with CG and BFGS algorithms are difficult to converge, with persistent oscillations in a few cases. Yet the FCP algorithm remains to deliver fast convergence to $|E_{Fermi} - \mu| \leq 10^{-3}$ eV within only two or three FCP steps except for the Fe case. In the Fe case, all three algorithms do not work well, but with Adaptive_lr (Figure 1) turned on, the FCP algorithm can deliver a fairly fast convergence to $|E_{Fermi} - \mu| \leq 10^{-3}$ eV in six FCP steps. Therefore, the FCP algorithm is a highly efficient and robust algorithm, which enables fast-converging FCP calculations that are resistant to numerical instability.

Note that the implicit electrolyte model of VASPsol renders the neutralizing background charge near the electrode surface (Figure S5), and the average electrostatic potential approaches zero in the middle of the electrolyte region (Figure S6), which implies that the neutralizing background charge well screens the surface dipoles and thus the middle of the electrolyte region well approximates the infinite deep of the electrolyte.

https://doi.org/10.1021/acs.jctc.3c00237
J. Chem. Theory Comput. XXXX, XXX, XXX−XXX

3.2. Practical Performance. Next, we test our FCP algorithm in constant-potential geometry optimization and BOMD for its practical performance. Duan and Xiao developed a constant-potential method for geometry optimization under the Python framework of ASE that treats N_e as an additional degree of freedom (DOF) of $\vec{r}_n$,[45] and the Python module is named "eAtoms",[46] which we use here as a reference for geometry optimization. The geometry optimization test calculations were conducted with the adsorption of CO molecule on the FeN_4/graphene single-atom catalyst, and the initial structure was set with an Fe−C distance of 2.00 Å. The constant-potential electronic state was optimized with our FCP algorithm and eAtoms for comparison, and the ionic positions were both optimized with the L-BFGS algorithm implemented in ASE.

Figure 3a shows that the optimized Fe−C distances for CO adsorption with eAtoms and our FCP methods are both 1.70 Å

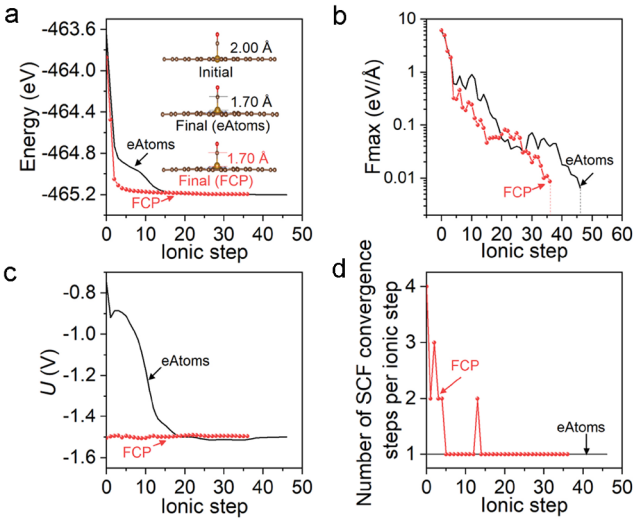

Figure 3. Constant-potential geometry optimization of CO adsorption on the FeN_4/graphene single-atom catalyst with eAtoms and FCP algorithms. (a) The grand-canonical energy, (b) the maximal force, (c) the potential U, and (d) the number of SCF convergence steps in each ionic step.

at $U = -1.5$ V; the optimized grand-canonical energies are marginally different because of the different methods to calculate the vacuum level in the two algorithms. Figure 3b shows that it takes 46 and 36 ionic steps for eAtoms and our FCP methods to converge the maximal force to within 0.01 eV/Å, respectively. The faster convergence of ionic positions by FCP arises from the more precise convergence of the electronic state characterized by U (Figure 3c) and thus more accurate forces for the open system at each ionic step. This embodies the key difference between the two methods; i.e., N_e and U are only converged in the last step with eAtoms because N_e is treated as a DOF the same as $\vec{r}_n$, but N_e and U are converged at every ionic step with FCP. Nevertheless, this leads to multiple SCF convergence steps in each ionic step with FCP, yet Figure 3d shows that only the first few ionic steps require more than one SCF convergence step with the FCP method. This is because the constant-capacitance approximation is tenable when the ionic positions do not vary much between two consecutive ionic steps and thus there is not a large fluctuation in N_e. Therefore, our FCP algorithm is highly efficient for FCP geometry optimization calculations.

Another widely used algorithm that delivers FCP calculations is JDFTx developed by Sundararaman et al.[18,43] The FCP calculations can be performed with JDFTx by adjusting N_e in an outer loop using the secant method (labeled as JDFTx-o) or by directly optimizing N_e in the convergence of the electronic state (labeled as JDFTx-i). We also test JDFTx-o and JDFTx-i with the constant-potential geometry optimization of CO adsorption on FeN_4/graphene, as shown in Figure S7a−c. All three algorithms (JDFTx-o, JDFTx-i, and FCP) converge U in every ionic step. JDFTx-i does so with only one electronic state convergence step per each ionic step, but JDFTx-o needs multiple electronic steps, while FCP requires two or three electronic steps for a few ionic steps and then only one electronic step for most of the ionic steps, similar to JDFTx-i. However, JDFTx-i requires a tight threshold of 10^{-7} eV for converging the electronic state, and the common threshold of 10^{-5} eV we aim to test here leads to the numerical instability in forces with JDFTx-i. Consequently, the maximal force with JDFTx-i cannot converge to within 0.01 eV/Å in 800 ionic steps, while it takes 64 and 36 ionic steps for JDFTx-o and FCP to converge, respectively. This implies that JDFTx-o and FCP are more robust than JDFTx-i. Therefore, the FCP algorithm has the advantages of both JDFTx algorithms; i.e., it is as robust as JDFTx-o for updating the ionic positions with accurate forces and as fast as JDFTx-i for converging the constant-potential electronic state.

The SJM method[20,25,28] implemented in GPAW[44] is also widely used to perform the GCE-DFT calculations, and thus we test it with the constant-potential geometry optimization of CO adsorption on FeN_4/graphene, as shown in Figure S8a−c. The SJM method demonstrates robustness similar to our FCP algorithm, and the Fermi level can converge in one to four SCF steps. The SJM method relies on the additional tight convergence condition that the differences between Fermi levels in the last three electronic steps of SCF should be smaller than 0.01 eV so that the numerical instability is greatly suppressed. It is a simple and efficient way to improve the robustness, and it works well for most of the cases. However, for some difficult cases such as the Fe surface slab, the tight convergence makes the SCF fail to converge in 1000 electronic steps.

We further test the FCP algorithm in performing the constant-potential BOMD simulations. The constant-potential BOMD calculations were first conducted with the molecular dynamics module in ASE using our FCP method as the calculator, and the model system we test is the coadsorption of a water molecule and a CO molecule on the FeN_4/graphene single-atom catalyst in the *NVT* ensemble with the temperature of 300 K controlled by the Nosé−Hoover thermostat. After 5 ps FCP BOMD calculations, the total energy, the temperature, and the charge are well-equilibrated, oscillating around the equilibrium values, and the U is precisely controlled at -1.5 ± 0.01 V in each MD step, as shown in Figure S9. The averaged number of SCF convergence steps per each ionic step is 1.36. Thus, the computational cost of this FCP-BOMD is just slightly more expensive than that of the normal constant-charge BOMD.

However, the potential should be fluctuating around the preset value by a potentiostat in the constant-potential MD simulations,[26,27,29] and N_e is updated according to Ohm's law:

https://doi.org/10.1021/acs.jctc.3c00237
J. Chem. Theory Comput. XXXX, XXX, XXX−XXX

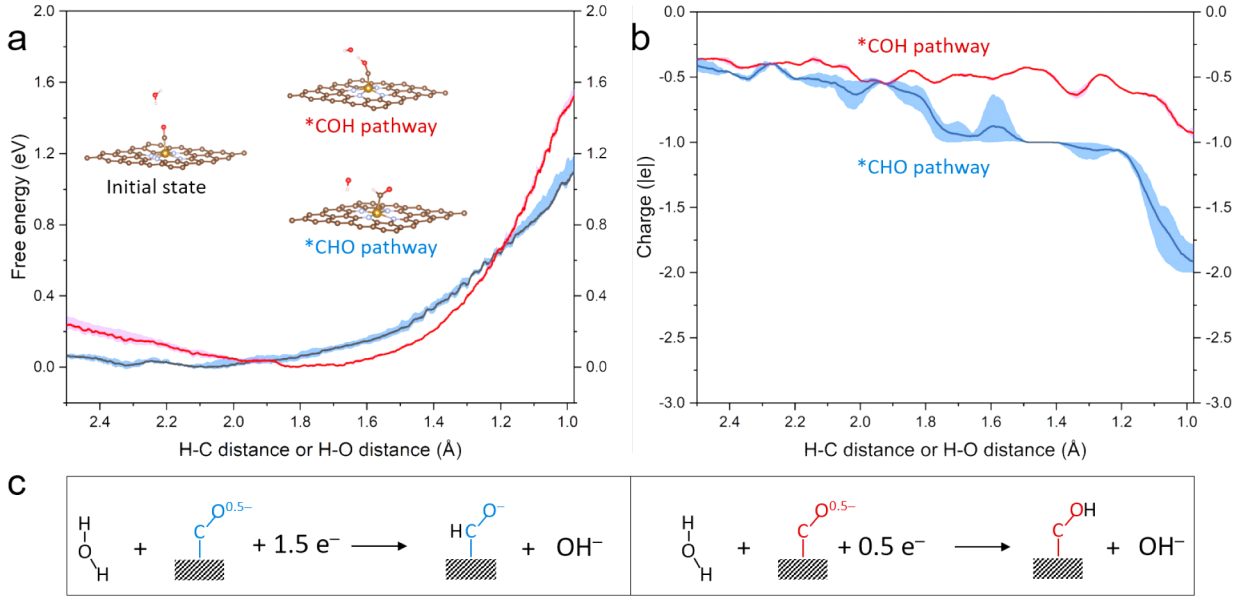

Figure 4. FCP steered-MD calculations of the two pathways for the electrochemical hydrogenation step of CO catalyzed by the FeN_4/graphene single-atom catalyst with H_2O acting as the proton source at $U = -1.5$ V. (a) The free energy surfaces and (b) the total charge evolution along the two pathways defined by corresponding CVs. (c) The possible reaction equations for the two pathways.

$$-e\frac{\Delta N_e}{\Delta t} = C_d(t)\frac{\Delta\left\{E_{Fermi}(t) - \left[\mu - R(t)\frac{e\Delta N_e}{\Delta t}\right]\right\}}{\Delta t} \quad (8)$$

where e is the elementary charge, Δt is the time step of the MD, ΔN_e is the difference in N_e between two MD steps, R is the resistance for charge transfer, and C_d is the differential capacitance defined as

$$C_d = e\frac{\partial N_e}{\partial E_{Fermi}} = eH^{-1} \quad (9)$$

where H is defined in eq 4 and is updated at every MD step in our FCP algorithm, so C_d can be explicitly calculated at every MD step. If we assume an ideal electron source (bath) that has no intrinsic resistance ($R = 0$), then eq 8 is simplified to

$$\frac{\Delta N_e}{\Delta t} = \frac{-H^{-1}(E_{Fermi} - \mu)}{\Delta t} \quad (10)$$

which is equivalent to eq 5. Thus, in order to perform the potentiostat MD simulations with fluctuating potentials, the only modification to adopt in our FCP algorithm is to restrict the iteration of N_e into one at every MD step; i.e., N_e is not necessarily converged to render $E_{Fermi} = \mu$. Nevertheless, eq 8 provides the driving force for the average of potential in the potentiostat MD simulations to converge to the given constant μ.

With the modification, we test the thermopotentiostat MD simulation with the coadsorption of water and CO on FeN_4/graphene starting from the thermal equilibrated state in Figure S9. The results in Figure S10 show that the fluctuation of potential here is very small, which is likely to arise from the assumption of $R = 0$. Thus, for computational simplicity, we keep using the FCP BOMD simulations without the potentiostat to showcase the following constant-potential enhanced-sampling BOMD simulations, so we do not need to sufficiently sample the fluctuating potenital and take the proper averages to obtain the free energy profiles. But we note that a potentiostat with a proper R is necessary for more realistic MD simulations.

Enhanced-sampling BOMD calculations have seen rapidly growing applications to the understanding of electrochemical reactions. Thus, we also tested the FCP algorithm in performing the FCP enhanced-sampling BOMD simulations. The test calculations were performed with the steered-MD method[47] using the ASE interface of PLUMED[48] nested with our FCP method as the calculator. The model electrochemical reaction we tested is the first electrochemical hydrogenation step of CO catalyzed by the FeN_4/graphene single-atom catalyst at $U = -1.5$ V. There are two possible pathways with the H atom transferred from water to the C atom (the CHO pathway) or to the O atom (the COH pathway) of the adsorbed CO. To study the kinetics of the two pathways, the distances between H in water and C or O of CO were chosen as the collective variables (CV) for the two pathways, and Figure 4a shows the free energy surfaces of the two pathways along the corresponding CVs. The CHO pathway has a free energy barrier of 1.12 eV, while the COH pathway has a larger free energy barrier of 1.53 eV. Thus, the first electrochemical hydrogenation step is more likely to occur via the CHO pathway on FeN_4/graphene, consistent with previous reports.[49−52] This may arise from that the CHO pathway can obtain more electrons (~1.5 e) from the electron reservoir (Figure 4b,c) and thus a larger electrochemical driving force. This case study illustrates the power of FCP enhanced-sampling BOMD simulations in understanding electrochemical reactions, and the significant difference in the charge evolution along the two pathways (Figure 4b) suggests that the constant-capacitance approximation may not be valid in general.

4. CONCLUSIONS

In summary, we developed a simple algorithm for performing efficient and robust FCP modeling of electrochemical interfaces. Our FCP algorithm is based on Newton's method with the polynomial fitting of the E_{Fermi}−N_e relationship to

https://doi.org/10.1021/acs.jctc.3c00237
J. Chem. Theory Comput. XXXX, XXX, XXX−XXX

obtain an analytical evaluation of $H \equiv \partial E_{\mathrm{Fermi}}/\partial N_e$. We demonstrated with constant-potential geometry optimization and BOMD calculations that our FCP algorithm is resistant to the numerical instability arising from the numerical errors in the SCF convergence of the electronic state with a common threshold of 10^{-5} eV, and it enables fast convergence to the preset electrochemical potential and renders accurate forces for updating the nuclear positions of an electronically open system, outperforming other available algorithms. Thus, it is an efficient and robust algorithm that can deliver effective FCP calculations with affordable computation costs.

Our FCP algorithm is currently implemented with the VASP interface of ASE, while it can be readily extended to using various computational codes as the underlying engine. Also, it can be easily combined with versatile packages such as PLUMED to perform constant-potential enhanced-sampling BOMD simulations including the blue-moon ensemble method and metadynamics, and it can be straightforwardly modified to perform the potentiostat MD simulations. With flexibility and versatility, our FCP algorithm can find a wide spectrum of applications in the modeling of chemistry at electrochemical interfaces.

■ ASSOCIATED CONTENT

Supporting Information

The Supporting Information is available free of charge at https://pubs.acs.org/doi/10.1021/acs.jctc.3c00237.

Additional computational details and supplementary figures (PDF)

■ AUTHOR INFORMATION

Corresponding Author

Hai Xiao − *Department of Chemistry, Tsinghua University, Beijing 100084, China;* orcid.org/0000-0001-9399-1584; Email: haixiao@tsinghua.edu.cn

Author

Zhaoming Xia − *Department of Chemistry, Tsinghua University, Beijing 100084, China; Department of Chemistry, Southern University of Science and Technology, Shenzhen 518055, China*

Complete contact information is available at: https://pubs.acs.org/10.1021/acs.jctc.3c00237

Notes

The authors declare no competing financial interest.

■ ACKNOWLEDGMENTS

This work was supported by the National Natural Science Foundation of China (Nos. 22122304 and 92261111), Tsinghua University Dushi Program, National Key Research and Development Project (2022YFA1503000), Tsinghua University Initiative Scientific Research Program (20221080065), and China Postdoctoral Science Foundation (2020M680507). We are grateful to the Center of High-Performance Computing at Tsinghua University, the Center for Computational Science and Engineering at SUSTech, and the CHEM High Performance Supercomputer Cluster (CHEM HPC) at the Department of Chemistry at SUSTech for providing computational resources.

■ REFERENCES

(1) Kohn, W. Nobel Lecture: Electronic structure of matter—wave functions and density functionals. *Rev. Mod. Phys.* **1999**, *71*, 1253−1266.

(2) Payne, M. C.; Teter, M. P.; Allan, D. C.; Arias, T. A.; Joannopoulos, J. D. Iterative minimization techniques for ab initio total-energy calculations: molecular dynamics and conjugate gradients. *Rev. Mod. Phys.* **1992**, *64*, 1045−1097.

(3) Anderson, A. B. Concepts and computational methods for the electrochemical interface and applications: past, present, and future. *Curr. Opin. Electrochem.* **2017**, *1*, 27−33.

(4) Sundararaman, R.; Vigil-Fowler, D.; Schwarz, K. Improving the accuracy of atomistic simulations of the electrochemical interface. *Chem. Rev.* **2022**, *122*, 10651−10674.

(5) Zhao, X.; Levell, Z. H.; Yu, S.; Liu, Y. Atomistic understanding of two-dimensional electrocatalysts from first principles. *Chem. Rev.* **2022**, *122*, 10675−10709.

(6) Nørskov, J. K.; Rossmeisl, J.; Logadottir, A.; Lindqvist, L.; Kitchin, J. R.; Bligaard, T.; Jónsson, H. Origin of the overpotential for oxygen reduction at a fuel-cell cathode. *J. Phys. Chem. B* **2004**, *108*, 17886−17892.

(7) Otani, M.; Hamada, I.; Sugino, O.; Morikawa, Y.; Okamoto, Y.; Ikeshoji, T. Electrode Dynamics from First Principles. *J. Phys. Soc. Jpn.* **2008**, *77*, No. 024802.

(8) Lozovoi, A. Y.; Alavi, A.; Kohanoff, J.; Lynden-Bell, R. M. Ab initio simulation of charged slabs at constant chemical potential. *J. Chem. Phys.* **2001**, *115*, 1661−1669.

(9) Cheng, T.; Xiao, H.; Goddard, W. A. Full atomistic reaction mechanism with kinetics for CO reduction on Cu(100) from ab initio molecular dynamics free-energy calculations at 298 K. *Proc. Natl. Acad. Sci. U.S.A.* **2017**, *114*, 1795−1800.

(10) Goldsmith, Z. K.; Calegari Andrade, M. F.; Selloni, A. Effects of applied voltage on water at a gold electrode interface from ab initio molecular dynamics. *Chem. Sci.* **2021**, *12*, 5865−5873.

(11) Letchworth-Weaver, K.; Arias, T. A. Joint density functional theory of the electrode-electrolyte interface: Application to fixed electrode potentials, interfacial capacitances, and potentials of zero charge. *Phys. Rev. B* **2012**, *86*, No. 075140.

(12) Fang, Y.-H.; Wei, G.-F.; Liu, Z.-P. Theoretical modeling of electrode/electrolyte interface from first-principles periodic continuum solvation method. *Catal. Today* **2013**, *202*, 98−104.

(13) Mathew, K.; Sundararaman, R.; Letchworth-Weaver, K.; Arias, T. A.; Hennig, R. G. Implicit solvation model for density-functional study of nanocrystal surfaces and reaction pathways. *J. Chem. Phys.* **2014**, *140*, No. 084106.

(14) Xiao, H.; Cheng, T.; Goddard, W. A. I.; Sundararaman, R. Mechanistic Explanation of the pH Dependence and Onset Potentials for Hydrocarbon Products from Electrochemical Reduction of CO on Cu (111). *J. Am. Chem. Soc.* **2016**, *138*, 483−486.

(15) Goodpaster, J. D.; Bell, A. T.; Head-Gordon, M. Identification of Possible Pathways for C-C Bond Formation during Electrochemical Reduction of CO_2: New Theoretical Insights from an Improved Electrochemical Model. *J. Phys. Chem. Lett.* **2016**, *7*, 1471−1477.

(16) Sundararaman, R.; Goddard, W. A.; Arias, T. A. Grand canonical electronic density-functional theory: Algorithms and applications to electrochemistry. *J. Chem. Phys.* **2017**, *146*, 114104.

(17) Mermin, N. D. Thermal Properties of the Inhomogeneous Electron Gas. *Phys. Rev.* **1965**, *137*, A1441−A1443.

(18) Sundararaman, R.; Letchworth-Weaver, K.; Schwarz, K. A.; Gunceler, D.; Ozhabes, Y.; Arias, T. A. JDFTx: Software for joint density-functional theory. *SoftwareX* **2017**, *6*, 278−284.

(19) Melander, M. M.; Kuisma, M. J.; Christensen, T. E. K.; Honkala, K. Grand-canonical approach to density functional theory of electrocatalytic systems: Thermodynamics of solid-liquid interfaces at constant ion and electrode potentials. *J. Chem. Phys.* **2019**, *150*, No. 041706.

(20) Melander, M. M. Grand canonical ensemble approach to electrochemical thermodynamics, kinetics, and model Hamiltonians. *Curr. Opin. Electrochem.* **2021**, *29*, 100749.

(21) Bonnet, N.; Morishita, T.; Sugino, O.; Otani, M. First-principles molecular dynamics at a constant electrode potential. *Phys. Rev. Lett.* **2012**, *109*, 266101.
(22) Bouzid, A.; Pasquarello, A. Redox Levels through Constant Fermi-Level ab Initio Molecular Dynamics. *J. Chem. Theory Comput.* **2017**, *13*, 1769−1777.
(23) Bouzid, A.; Pasquarello, A. Atomic-Scale Simulation of Electrochemical Processes at Electrode/Water Interfaces under Referenced Bias Potential. *J. Phys. Chem. Lett.* **2018**, *9*, 1880−1884.
(24) Zhao, X.; Liu, Y. Origin of selective production of hydrogen peroxide by electrochemical oxygen reduction. *J. Am. Chem. Soc.* **2021**, *143*, 9423−9428.
(25) Kastlunger, G.; Lindgren, P.; Peterson, A. A. Controlled-Potential Simulation of Elementary Electrochemical Reactions: Proton Discharge on Metal Surfaces. *J. Phys. Chem. C* **2018**, *122*, 12771−12781.
(26) Deißenbeck, F.; Freysoldt, C.; Todorova, M.; Neugebauer, J.; Wippermann, S. Dielectric Properties of Nanoconfined Water: A Canonical Thermopotentiostat Approach. *Phys. Rev. Lett.* **2021**, *126*, 136803.
(27) Deißenbeck, F.; Wippermann, S. Dielectric Properties of Nanoconfined Water from Ab Initio Thermopotentiostat Molecular Dynamics. *J. Chem. Theory Comput.* **2023**, *19*, 1035−1043.
(28) Melander, M.; Wu, T.; Honkala, K. Constant Inner Potential DFT for Modelling Electrochemical Systems under Constant Potential and Bias. *ChemRxiv*, March 1, 2023, ver. 3. DOI: 10.26434/chemrxiv-2021-r621x-v3.
(29) García-Morales, V.; Krischer, K. Fluctuation enhanced electrochemical reaction rates at the nanoscale. *Proc. Natl. Acad. Sci. U.S.A.* **2010**, *107*, 4528−4532.
(30) Franco-Pérez, M.; Ayers, P. W.; Gázquez, J. L.; Vela, A. Thermodynamic responses of electronic systems. *J. Chem. Phys.* **2017**, *147*, No. 094105.
(31) Domínguez-Flores, F.; Melander, M. M. Approximating constant potential DFT with canonical DFT and electrostatic corrections. *J. Chem. Phys.* **2023**, *158*, 144701.
(32) Trasatti, S. The absolute electrode potential: an explanatory note (Recommendations 1986). *Pure Appl. Chem.* **1986**, *58*, 955−966.
(33) Wentzcovitch, R. M.; Martins, J. L.; Allen, P. B. Energy versus free-energy conservation in first-principles molecular dynamics. *Phys. Rev. B* **1992**, *45*, 11372−11374.
(34) Weinert, M.; Davenport, J. W. Fractional occupations and density-functional energies and forces. *Phys. Rev. B* **1992**, *45*, 13709−13712.
(35) Larsen, A. H.; Mortensen, J. J.; Blomqvist, J.; Castelli, I. E.; Christensen, R.; Dułak, M.; Friis, J.; Groves, M. N.; Hammer, B.; Hargus, C.; Hermes, E. D.; Jennings, P. C.; Jensen, P. B.; Kermode, J.; Kitchin, J. R.; Kolsbjerg, E. L.; Kubal, J.; Kaasbjerg, K.; Lysgaard, S.; Maronsson, J. B.; Maxson, T.; Olsen, T.; Pastewka, L.; Peterson, A.; Rostgaard, C.; Schiøtz, J.; Schütt, O.; Strange, M.; Thygesen, K. S.; Vegge, T.; Vilhelmsen, L.; Walter, M.; Zeng, Z.; Jacobsen, K. W. The atomic simulation environment—a Python library for working with atoms. *J. Phys.: Condens. Matter.* **2017**, *29*, 273002.
(36) Kresse, G.; Hafner, J. Ab initio molecular dynamics for liquid metals. *Phys. Rev. B* **1993**, *47*, 558−561.
(37) Kresse, G.; Furthmüller, J. Efficiency of ab-initio total energy calculations for metals and semiconductors using a plane-wave basis set. *Comput. Mater. Sci.* **1996**, *6*, 15−50.
(38) Kresse, G.; Furthmüller, J. Efficient iterative schemes for ab initio total-energy calculations using a plane-wave basis set. *Phys. Rev. B* **1996**, *54*, 11169−11186.
(39) Kresse, G.; Joubert, D. From ultrasoft pseudopotentials to the projector augmented-wave method. *Phys. Rev. B* **1999**, *59*, 1758−1775.
(40) *VASPsol*. https://github.com/henniggroup/VASPsol (accessed 2022-04-30).
(41) Mathew, K.; Kolluru, V. S. C.; Mula, S.; Steinmann, S. N.; Hennig, R. G. Implicit self-consistent electrolyte model in plane-wave density-functional theory. *J. Chem. Phys.* **2019**, *151*, 234101.
(42) Gunceler, D.; Letchworth-Weaver, K.; Sundararaman, R.; Schwarz, K. A.; Arias, T. A. The importance of nonlinear fluid response in joint density-functional theory studies of battery systems. *Model. Simul. Mat. Sci. Eng.* **2013**, *21*, No. 074005.
(43) Sundararaman, R. *jdftx*. https://github.com/shankar1729/jdftx (accessed 2021-12-30).
(44) Mortensen, J. J.; Hansen, L. B.; Jacobsen, K. W. Real-space grid implementation of the projector augmented wave method. *Phys. Rev. B* **2005**, *71*, No. 035109.
(45) Duan, Z.; Xiao, P. Simulation of potential-dependent activation energies in electrocatalysis: mechanism of O-O bond formation on RuO_2. *J. Phys. Chem. C* **2021**, *125*, 15243−15250.
(46) Xiao, P. *Electrochemical-barrier*. https://github.com/penghao-xiao/Electrochemical-barrier (accessed 2022-04-30).
(47) Grubmüller, H.; Heymann, B.; Tavan, P. Ligand binding: molecular mechanics calculation of the streptavidin-biotin rupture force. *Science* **1996**, *271*, 997−999.
(48) Sucerquia, D.; Parra, C.; Cossio, P.; Lopez-Acevedo, O. Ab initio metadynamics determination of temperature-dependent free-energy landscape in ultrasmall silver clusters. *J. Chem. Phys.* **2022**, *156*, 154301.
(49) Zhang, B.; Zhang, B.; Jiang, Y.; Ma, T.; Pan, H.; Sun, W. Single-atom electrocatalysts for multielectron reduction of CO_2. *Small* **2021**, *17*, 2101443.
(50) Cao, S.; Wei, S.; Wei, X.; Zhou, S.; Chen, H.; Hu, Y.; Wang, Z.; Liu, S.; Guo, W.; Lu, X. Can N, S Cocoordination Promote Single Atom Catalyst Performance in CO2RR? Fe-N2S2 Porphyrin versus Fe-N4 Porphyrin. *Small* **2021**, *17*, 2100949.
(51) Zhang, X.; Li, F.; Wang, J.; Zhao, H.; Yu, X.-F. Strategy for improving the activity and selectivity of CO_2electroreduction on flexible carbon materials for carbon-neutral. *Appl. Energy* **2021**, *298*, 117196.
(52) Yang, Y.; Li, J.; Zhang, C.; Yang, Z.; Sun, P.; Liu, S.; Cao, Q. Theoretical Insights into Nitrogen-Doped Graphene-Supported Fe, Co, and Ni as Single-Atom Catalysts for CO_2Reduction Reaction. *J. Phys. Chem. C* **2022**, *126*, 4338−4346.

https://doi.org/10.1021/acs.jctc.3c00237
J. Chem. Theory Comput. XXXX, XXX, XXX−XXX